Handling Radar Cross-Section Performance in Monitoring Vital Signs Under Constraint Conditions

Faheem Khan[1]*, Saleh M. Sherazi[2], Naeem Khan[1]*, Imran Ashraf[3]* and Fahad Khan[1]

[1]Lab STICC, Communications Engineering, UBO, Brest, France, [2]Electrical Engineering Department, UET Bannu Campus, University of Engineering and Technology, Bannu, Pakistan, [3]Electrical Engineering Department, HITEC, Islamabad, Pakistan

Two vital signs including heartbeat and respiratory rate are monitored in this work under two constraint situations; namely noise disturbance and intermittent observations. The existing scheme for finding, measuring and monitoring vital signs was Fourier Transform which could not deal with non-stationary process. As an alternative, the Wavelet Transform is used in this work which is equally applicable to both stationary and non-stationary processes. Additionally, the loss of output data may result in crucial implications in observing vital signs. Formerly, only un-interrupted data has been amalgamated in tracing vital signs. A novel adaptive ARMA-based scheme is proposed to obtain optimum estimated results in the presence of the above two critical scenarios. Simulation results obtained on real (practical) data show that the ARMA-based model produces similar vital signs as shown by clean and un-distorted data. It is shown that the proposed ARMA-based algorithm improves the breathing rate accuracy by 0.3% and heart rate accuracy by 2.5% as compared to the existing AR-based vital signal reconstruction algorithm.

Keywords: vital signs, radar-cross section, ARMA-model, kalman filtering, intermittent observations

1 INTRODUCTION

Formerly, the Ultra-Wide Band (UWB) standards were allowed unauthorized operation in the area of 3.1–10.6 GHz (Fernandes and Wentzloff, 2010). Since the authorization of UWB by the Federal Communication Commission in 2002, Ultra-Wide Band has a huge contribution in wireless communication (Fontana, 2004; Li et al., 2010; Choliz et al., 2011) and radar sensor applications (Oziel et al., 2017; Fear et al., 2002; Buehrer et al., 2003; Lazaro et al., 2009; Thiel et al., 2010). Ultra-Wide Band has many advantages namely strength in harsh environments, location accuracy and high penetration capability (Briso et al., 2019), etc. With the help of IR-UWB radar, both micro and macro movements can be sensed inside the human body (Staderini, 2002). For such reasons, UWB has large applications in the medical field because it consumes less power and provides higher extensional quality (Grewal and Andrews, 2001). The monitoring of vital signs has acquired greater attention in case of surveillance of non-communicable patients and the search for people after natural disasters (Khan et al., 2020; Le, 2020; Yang et al., 2020). **Figure 1** shows the experimental setup for this work. The patient is sitting in front of the radar in a range of around 1 m. The radar signal is back scattered from the human body as well as the background environment. The background signal is considered as clutter and removed using a moving averaging filter while the moving part of the signal contains the displacement caused by the human lungs and heart. These periodic motions are extracted from the signal using signal processing techniques explained in **Section 2** of this work.

FIGURE 1 | IR-UWB radar working principle.
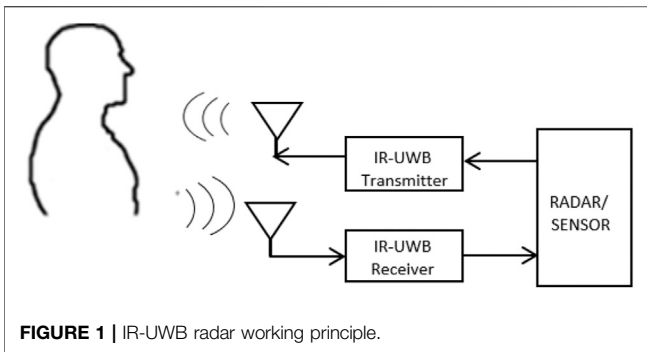
The standard model of static UWB Cramer et al., (2002) can be expressed as

$$y(\alpha) = \sum_{j=1}^{M} \rho_j \varphi_j \left(\alpha - n_j\right) \qquad (1)$$

The extended version used in the multi-channel UWB model (Liu et al., 2019), is developed as follows:

$$y(t, \alpha) = \sum_{j=1}^{M} \rho_j(t) \varphi_j \left(\alpha - n_j(t)\right) \qquad (2)$$

In the above equations, α is the time delay and t shows time instance. The most scattered M-line overlap is the channel model parameter $y(t, \alpha)$. The time of arrival of the path is specified by j which can be accessed by $n_j(t)$. $\rho_j(t)$ represents the magnitude of the path and $\varphi_j(\alpha - n_j(t))$ shows the path waveform. Previously, the Fourier Transform (FT) has remained a dominant scheme for vital sign monitoring of patients (Khan et al., 2020). Although many researchers use FT algorithm for respiration and heart rate measurement using band pass filtering. However, sometimes respiration signal generates harmonics at integral multiples of the breathing frequency and some of the harmonics overlap the heart rate frequency region. Since the respiration movement has higher magnitude than heart rate so it becomes difficult or impossible to extract heart rate using simple band pass filtering. For such reasons, FT is not a suitable choice for analyzing non-stationary data (Khan et al., 2018). Therefore, it is still highly desirable to introduce a method that can simultaneously provide information about frequency localization and time localization. In this concern, Short Term FT (STFT) fulfills the need for synchronous frequency and time information (Khan and Cho, 2017), Employing STFT can lead to decision problems such as the selection of window size and time resolution (Khan et al., 2020). Another essential dilemma of STFT is its immutable window size. Due to this, narrow windows provide high time resolution, but frequency accuracy is low, while wide windows provide improved frequency accuracy but poor time accuracy. A continuous Wavelet Transform (WT) has been developed as an alternative way to convert short time FT to solve the above-mentioned problem. An important characteristic of WT is that it provides result even with variable window size, hence

extracting information through WT is much attractive than FT (Shen et al., 2018).

An important challenge in this field is to deal with the intermittent or anomalous data that can occur for a variety of reasons. No doubt, the availability of output data for processing purposes is necessary for majority of communication systems. In this connection, it is perhaps more crucial to consider the possible consequences of interrupted or intermittent data in case of diagnosis of a patient. The main cause of data loss occurs when the patient's position is slightly offset and does not accurately face the radar/sensor for a period of time, so the Radar Cross Section (RCS) with a narrow beam width in front of the antenna is reduced, resulting in intermittent measurement. In this case, we ignore the outliers and treat them as missing data. This paper also aims to identify such data loss and propose remedial measures in the form of robust algorithms. In a related work (Gu et al., 2013), a radar sensor system with camera aided random body movement detection and tracking was presented. However, it is expensive to use additional camera for tracking the body movement. In (Cardillo et al., 2021), only one radar sensor is used for both vital signs and motion detection, however, the motion considered in that work is due to the radar sensor and human body motion was not considered in that work. In our presented work, the source of the interrupted or intermittent data is not important. The main contributions of this paper are best explained in schematic shown in **Figure 2**, which also illustrates the strategy used in this paper.

It is necessary to state that data loss can be recovered through many techniques which mainly depends on the structure or pattern available in the data. As assumed in (Khan et al., 2019), this paper assumes that the processing time interval is limited enough so that the signal can be seen as being almost stationary. The main contribution of this paper is that it proposes an algorithm based on WT and ARMA model. A proper wavelet is carefully selected to detect the breathing and heart rate signal in the radar back scattered signal. An ARMA model is proposed for predicting the missing data that may cause inaccuracy in the vital measurement process. Another contribution is that this work is based on real radar data which was collected in a university hospital from a patient.

The structure of this paper is given as: **Section 2** describes the details of existing techniques for data Loss. **Section 3** contains Auto-Regressive Moving Average (ARMA) based model and Wavelet Transform. **Section 4** describes the scenario when there is no data loss in the measurement of vital signs. **Section 5** introduces the case of data loss during vital signs measurement. **Section 6** includes measurement recovery through AR-based model. **Section 7** includes loss recovery measurement through proposed ARMA-based model. Finally, **Section 7** concludes this work and discusses possible future work in this research area.

It is worth mentioning that all the results obtained in this paper are based on radar technology using Xethru X4 (Novelda,

FIGURE 2 | Graphical representation of the paper strategy.
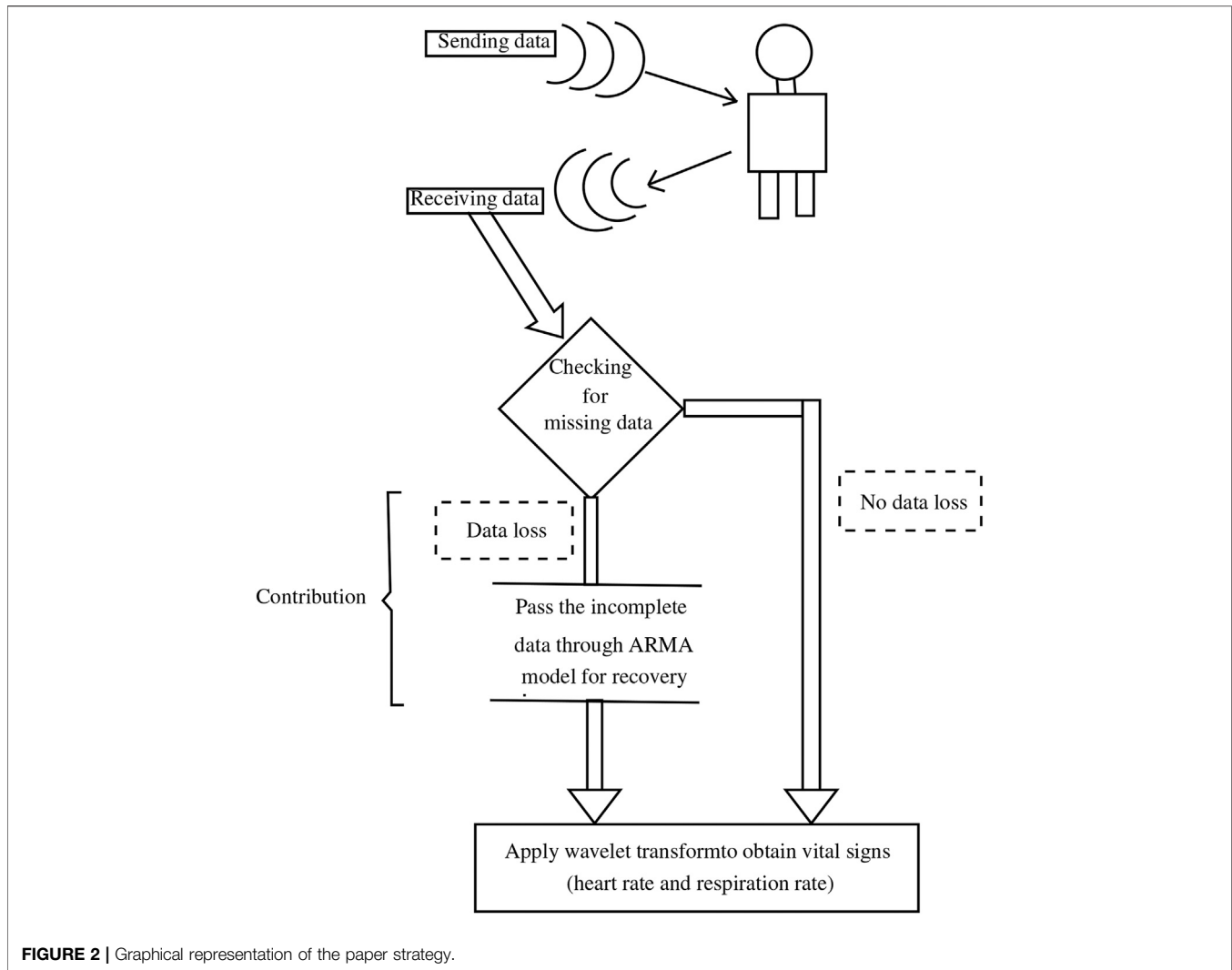
Norway) sensor (Andersen et al., 2017). The central frequency of this radar sensor is 8.7 GHz with a bandwidth of 2.9 GHz. The output power, pulse repetition frequency and beam width parameters are -12.6 dB m, 400 MHz and 65°, respectively. The sensor has a very fine range resolution of 6.4 cm. It consists of one transmitter and one receiver antenna. The radar sensor was connected to PC through USB cable. The radar back scattered signals were processed in the PC using Matlab software.

2 EXISTING TECHNIQUES FOR PACKET LOSS

Several mechanisms exist which handle data loss, such as Open-Loop Estimation (OLE) and Compensated Closed-loop Estimation (CCLE). In the following sub-sections, these algorithms are briefly elaborated with associated shortcomings.

2.1 Open-Loop Estimation

It is a very simpler scheme devised for data loss and has been employed in numerous application. The basic mechanism of OLE is discussed as follows:

For a discrete-time LTI system, with dynamics

$$x_{k+1|k} = Ax_{k|k} + Bu_k + \omega_k$$
$$y_{k+1|k} = \vartheta_{k+1}(H\ x_{k+1} + \theta_{k+1})$$

the standard Kalman filtering estimates $x_{k+1|k}$ in two steps namely prediction-cycle and update-cycle. Contrary to the standard Kalman filter, the OLE is summarized in **Algorithm 1**. OLE is a fast algorithm for signal recovery, however, it may cause divergence in case of adequate data loss and sudden crusts and troughs may appear in recovered signal. Further, it may be difficult to reach the steady state after resumption of the original signal. Due to these limitations, series-based algorithms are proposed in the next section to predict the missing part of the signal.

Algorithm 1. Open loop estimation

Initialize $\mathbf{x}_{0|0}, \mathbf{u}_0, \boldsymbol{\theta}_0, \boldsymbol{\epsilon}_0, \mathbf{P}_{0|0}$ and $k = 1, N =$ number of samples

while $k \leq N$ **do**
    Prediction cycle
    $\mathbf{x}_{k+1|k} = \mathbf{A}\mathbf{x}_{k|k} + \mathbf{B}\mathbf{u}_k$: State estimation
    $\mathbf{P}_{k+1|k} = \mathbf{A}\mathbf{P}_{k|k}\mathbf{A}^T + \mathbf{Q}_k$: Error covariance

    Time update step
    $k \leftarrow k + 1$

    No information signal: $\mathbf{y}_{k+1|k} = \vartheta_k(\mathbf{H}\mathbf{x}_{k+1} + \boldsymbol{\theta}_{k+1})$ with $\vartheta_k = 0$

    Update step
    $\mathbf{x}_{k+1|k+1} = \mathbf{x}_{k+1|k}$: State estimation
    $\mathbf{P}_{k+1|k+1} = \mathbf{P}_{k+1|k}$: Error covariance

end while

2.2 Series-Based Algorithms

The compensated closed-loop scheme has efficiently reconstructed the missing data and promising estimation results have been achieved. The recent achievements obtained through this model can be seen in Khan et al. (2013) and Khan et al. (2010). Data loss occurred in series which may have any trend are more expected to be recovered through Autoregressive (AR) series. These series include AR, MA, and ARMA to name but a few. Human vital signal possess a periodic trend, therefore it can be recovered through AR series. AR model employed for compensation of measurement has the mathematical formulation as

$$\bar{y}_k = \sum_{j=1}^{W} \gamma_j y_{k-j} \tag{3}$$

where γ_j are prediction coefficients, y_{k-j} are previous samples of observation stored in memory stack, and W is the order of linear prediction filter. The optimum values of the prediction coefficients can be computed as

$$A_r = R_r^{-1} r_r \tag{4}$$

where,

$$A_r = \begin{bmatrix} \gamma_1 & \gamma_2 & \ldots\ldots\ldots & \gamma_W \end{bmatrix}^T \tag{5}$$

is the vector containing the unknown coefficients,

$$r_i = [r_r[1] \ldots\ldots\ldots\ldots\ldots r_r[W]]^T \tag{6}$$

is the linear prediction array and

$$R_r = \begin{bmatrix} R_r[0] & R_r[1] & \ldots & R_r[W-1] \\ R_r[1] & R_r[0] & \ldots & R_r[W-2] \\ \vdots & \vdots & \ddots & \vdots \\ R_r[W-1] & R_r[W-2] & \ldots & R_r[0] \end{bmatrix} \tag{7}$$

is the auto-correlation matrix. The elements of linear prediction array and auto-correlation matrix can be obtained as

$$E\left[y_{k-j}^T y_{k-i}\right] = \begin{cases} R_r[0], & \text{if } j = i; \\ R_r[|j - i|], & \text{if } j \neq i. \end{cases} \tag{8}$$

With the help of **Equation 4**, the optimal values of linear prediction coefficients are computed which are then employed in finding the
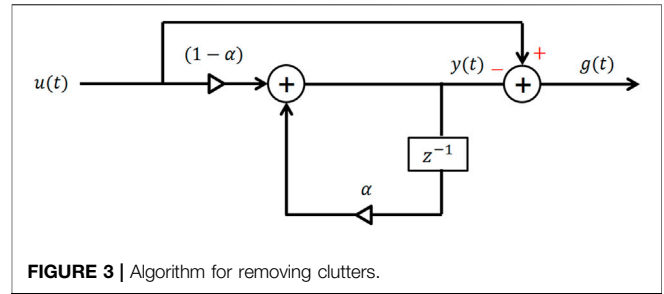

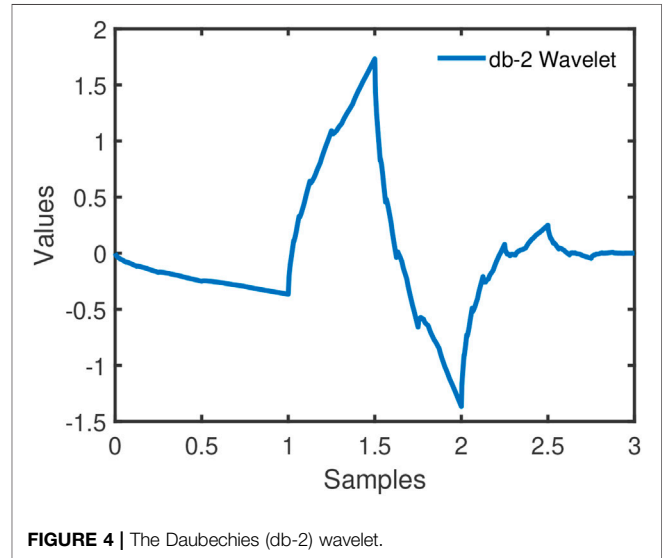**FIGURE 3 |** Algorithm for removing clutters.

FIGURE 4 | The Daubechies (db-2) wavelet.

lost samples using **Eq. 3**. The AR model uses only measurement vector for linear prediction coefficient (LPC) computation, however, in our proposed ARMA-based reconstruction of vital signal the input as well as measurement vector are used for LPC computation which improves the prediction accuracy.

3 PROPOSED ARMA-BASED MODEL AND WAVELET TRANSFORM

In the subsequent section, we present the proposed model which is based on ARMA series.

3.1 Proposed ARMA-Based Model

The data recovery scheme used in this paper is based on ARMA based model. The mathematical description of ARMA based model is as follows;

$$\bar{y}_k = \sum_{j=1}^{W} \gamma_j y_{k-j} + \sum_{j=1}^{W} \delta_j u_{k-j} \tag{9}$$

where,

In the above equations, W represent filter linear prediction order, y_{k-j} shows sensor readings and u_{k-j} shows the input signal to the plant/system. The symbols γ_j and δ_j represent weights given

to measurements and input respectively. The error resulting by this compensating vector would be

$$\mathbf{e}_k = \mathbf{y}_k - \bar{\mathbf{y}}_k \tag{10}$$

where $\mathbf{y}_k$ is the actual observation vector. In order to compute linear prediction coefficients efficiently, the cost function consists of mean square prediction error as;

$$J \overset{\text{def}}{=} E\left[\mathbf{e}_k^2\right] \tag{11}$$

or

$$J = E\left[\left(\mathbf{y}_k - \sum_{j=1}^{W}\boldsymbol{\gamma}_j \mathbf{y}_{k-j} - \sum_{j=1}^{W}\boldsymbol{\delta}_j \mathbf{u}_{k-j}\right)^2\right] \tag{12}$$

In order to find the optimal value of $\boldsymbol{\gamma}_j$, which will result in the minimum cost function, we proceed as

$$\frac{\partial J}{\partial \gamma_j} = 2E\left[\left(\mathbf{y}_k - \sum_{j=1}^{W}\boldsymbol{\gamma}_j \mathbf{y}_{k-j} - \sum_{j=1}^{W}\boldsymbol{\delta}_j \mathbf{u}_{k-j}\right)\mathbf{y}_{k-i}\right] = 0 \tag{13}$$

$$E\left[\boldsymbol{\gamma}_j \sum_{j=1}^{W}\mathbf{y}_{k-j}\mathbf{y}_{k-i}\right] + E\left[\boldsymbol{\delta}_j \sum_{j=1}^{W}\mathbf{u}_{k-j}\mathbf{y}_{k-i}\right] = E\left[\mathbf{y}_k\mathbf{y}_{k-i}\right] \tag{14}$$

Let

$$\begin{aligned}
E\left[\mathbf{y}_k\mathbf{y}_{k-j}\right] &= \mathbf{l}_1 \\
E\left[\mathbf{y}_{k-j}\mathbf{y}_{k-i}\right] &= \mathbf{L}_1 \\
E\left[\mathbf{u}_{k-j}\mathbf{y}_{k-i}\right] &= \mathbf{L}_2
\end{aligned} \tag{15}$$

Substituting **Eq. 15** in **Eq. 14** will result in

$$\mathbf{L}_1\boldsymbol{\gamma}_j + \mathbf{L}_2\boldsymbol{\delta}_j = \mathbf{l}_1 \tag{16}$$

In the similar way, the optimal value of $\boldsymbol{\delta}_j$ are calculated as

$$\frac{\partial J}{\partial \delta_j} = 2E\left[\left(\mathbf{y}_k - \sum_{j=1}^{W}\boldsymbol{\gamma}_j \mathbf{y}_{k-j} + \sum_{j=1}^{W}\boldsymbol{\delta}_j \mathbf{u}_{k-j}\right)\mathbf{u}_{k-i}\right] = 0 \tag{17}$$

$$E\left[\boldsymbol{\gamma}_j \sum_{j=1}^{W}\mathbf{y}_{k-j}\mathbf{u}_{k-i}\right] + E\left[\boldsymbol{\delta}_j \sum_{j=1}^{W}\mathbf{u}_{k-j}\mathbf{u}_{k-i}\right] = E\left[\mathbf{y}_k\mathbf{u}_{k-i}\right] \tag{18}$$

$$\begin{aligned}
E\left[\mathbf{y}_k\mathbf{u}_{k-j}\right] &= \mathbf{l}_2 \\
E\left[\mathbf{y}_{k-j}\mathbf{u}_{k-i}\right] &= \mathbf{L}_3 \\
E\left[\mathbf{u}_{k-j}\mathbf{u}_{k-i}\right] &= \mathbf{L}_4
\end{aligned} \tag{19}$$

Substituting **Eq. 19** in **Eq. 18** will result in

$$\mathbf{L}_3\boldsymbol{\gamma}_j + \mathbf{L}_4\boldsymbol{\delta}_j = \mathbf{l}_2 \tag{20}$$

Multiply **Eq. 16** by $\mathbf{L}_4$ and **Eq. 20** by $\mathbf{L}_2$ and solve simultaneously i.e.

$$\boldsymbol{\gamma}_j = [\mathbf{L}_1\mathbf{L}_4 - \mathbf{L}_2\mathbf{L}_3]^{-1}[\mathbf{L}_4\mathbf{l}_1 - \mathbf{L}_2\mathbf{l}_2] \tag{21}$$

Multiply **Eq. 16** by $\mathbf{L}_3$ and **Eq. 20** by $\mathbf{L}_1$ and solve simultaneously i.e.

$$\boldsymbol{\delta}_j = [\mathbf{L}_2\mathbf{L}_3 - \mathbf{L}_1\mathbf{L}_4]^{-1}[\mathbf{L}_3\mathbf{l}_1 - \mathbf{L}_1\mathbf{l}_2] \tag{22}$$

Using **Eq. 21** and **Eq. 22**, the auxiliary measurement vector can be reconstructed through a model depicted in **Eq. 9**.

Algorithm 2. Filter order selection

Calculate $e_m(k-1) = max(e_i)$ where $e_i = y_i - \bar{y}_i \; \forall i = (1, 2, 3, \ldots\ldots, k-1)$

Initialize $j = 1$, then compute $l_1, l_2, L_1, L_2, L_3, L_4$

while $j \leq W$ **do**
   Obtain $\bar{y}_k$ using Equation 9

   Compute measurement update state on the basis of compensated vector

   $\bar{e}_k = \bar{y}_k - y_k$

   if $\bar{e}_k \leq e_m(k-1)$ **then**

      $W \leftarrow j$: order of LP filter

   else

      $j \leftarrow j + 1$

   end if

end while

Additionally, it is fundamental to decide the optimal value of prediction filter order W. Various schemes can be proposed to compute this important parameter. The importance of this parameter can be judged from the fact that a high value of W will take a large number of samples to reconstruct the missing sample and hence will consume more computational time. On the other hand, a smaller value of W may generate degraded results at the price of less computational time. Hence, it is a task for the designer to devise an optimal value of W to result in optimum achievements. In **Algorithm 2**, a simple and straightforward mechanism is proposed to decide the order of prediction filter, when samples start missing at k*th* instance.

3.2 Clutter Removal and Wavelet Transform

Due to the vital limitations of FT-based scheme, this paper aims to employ Wavelet Transform (WT) as an alternate, and hence, a brief review of WT is considered to be beneficial. IR-UWB radar surrounds the body under study. From the patient's body, constant reflected rays are received. The received signal from the body contains data, stored in an $m \times n$ matrix, where m is the sample size in the slow time and n represents the occurrence of the sample in the fast time. First, search for the column with the highest power. For clutter cancellation, the signal must pass through a filter, such as a notch filter (Sifuzzaman et al., 2009; Chia et al., 2005; Grewal and Andrews, 2001. From a graphical perspective, the clutter removal process can be seen in **Figure 3**. Mathematically, the separator can be described as follows (Wang et al., 2017.

$$y(t) = a y(t-1) + (1-a)u(t) \tag{23}$$
$$g(t) = u(t) - y(t) \tag{24}$$

where, y(t), u(t) and g(t) represent the clutter signal, original signal and clutter free signal respectively.

The Wavelet coefficients are achieved by applying WT on the clutter free signal. In addition, the mother Wavelet used in this
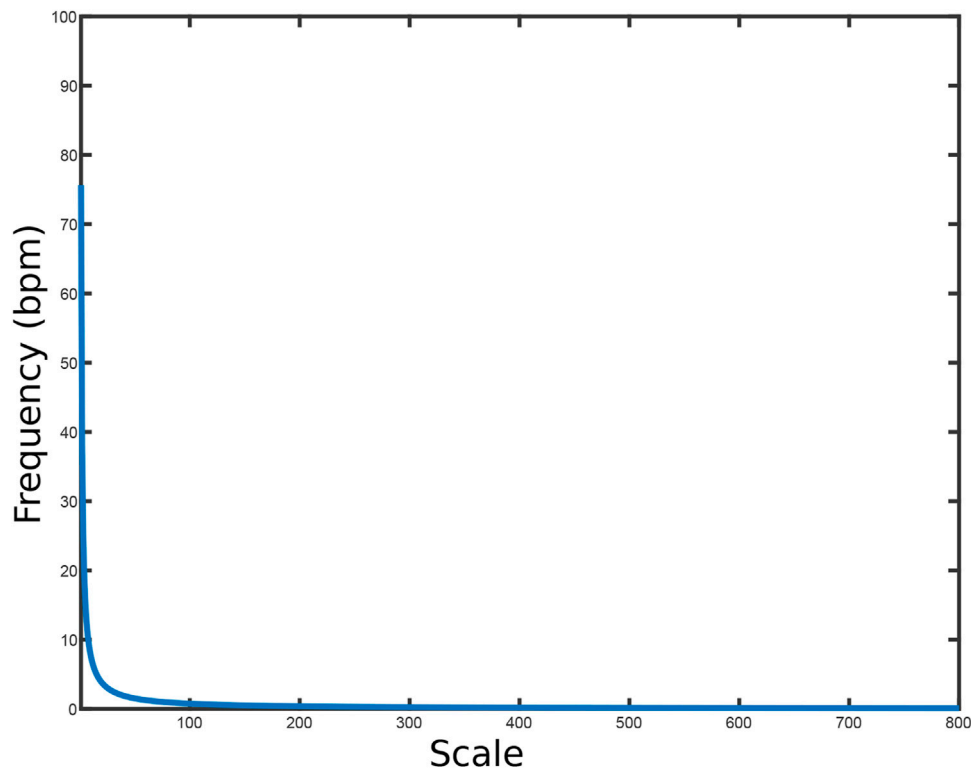
FIGURE 5 | Frequency plot of Daubechies (db-2) Wavelet.

case is Daubechies-2. The pictorial view of db-2 Wavelet is given in **Figure 4**.

The Wavelet coefficients are obtained after the Wavelet is applied to the clutter-free signal. It needs to be noted that the Wavelet coefficients, when plotted on Energy-Spectral Density (ESD) graph, provide scale value. Another commending feature of Wavelet transform is that it gives Scale-to-Frequency graphs (for example **Figure 5**) Tariq et al. (2017). So, core objective of **Figure 5**, is to locate the corresponding frequency of scale factor related to heart rate or respiration rate. This strategy is adopted for the detection of vital signs in the following four scenarios:

1. Analysis of Normal Scenario (discussed in **Section 4**)
2. Consequences of data loss (discussed in **Section 5**)
3. Analysis after Recovery of Data Loss through AR-based Model (discussed in **Section 6**)
4. Analysis after Recovery of Data Loss through ARMA-based model (discussed in **Section 7**)

4 ANALYSIS OF NORMAL SCENARIO

Initially, smoothly arrived data has been analyzed which will serve as a baseline for comparison. After removing the clutter by any convenient method (such as notch filter), the clutter-free signal will consist of two parts (heart rate and respiration rate), and the Wavelet coefficients are obtained by applying Wavelet transform to the clutter-free signal. This results in the scale-frequency plot

depicted in **Figure 5**. From this figure, the frequency can be found which corresponds to the density of the Wavelet coefficients.

In the same way, applying WT to the signal received without any missing sample from the patient gives the result shown in **Figure 6**, which contains two sub-results. Upper figure shows the analysis signal in the survey. The scalogram chart in lower figure is Daubechies (db-2) Wavelet (Tariq et al., 2017). It is important to note that in normalized case, the heart rate is between 60–120 beats/min, which is related to the scale value of 35–75. The appropriate measurement range is chosen for the heart rate and the selected scale, where Wavelet coefficients have the largest low energy, as shown in **Figure 6**. For heart rate, the approximate scale has a value of 42 (continuous pink line in **Figure 6**), which corresponds to a frequency of 1.801 Hz in **Figure 7**. The heart rate can be calculated as $1.801 \times 60 = 108.08$ bpm.

In the same way, the range of respiration rate lies between 10–30 bpm, which corresponds to a scale value of 150–450 (Chia et al., 2005; Wang et al., 2017). The respiration rate scale can be selected by measuring the maximum spectral energy within these ranges. The generated scale value associated with the loss-free data is 350 as shown in **Figure 8**. The 350 scale value corresponds to a frequency of 0.2161 Hz in **Supplementary Figure S1**. Therefore, the heart rate can be calculated as 12.96 = (0.2161*60) bpm. There are two readings, obtained from uninterrupted signal, which are:

1. Respiration rate = 12.96 bpm.
2. Heart rate = 108.08 bpm.

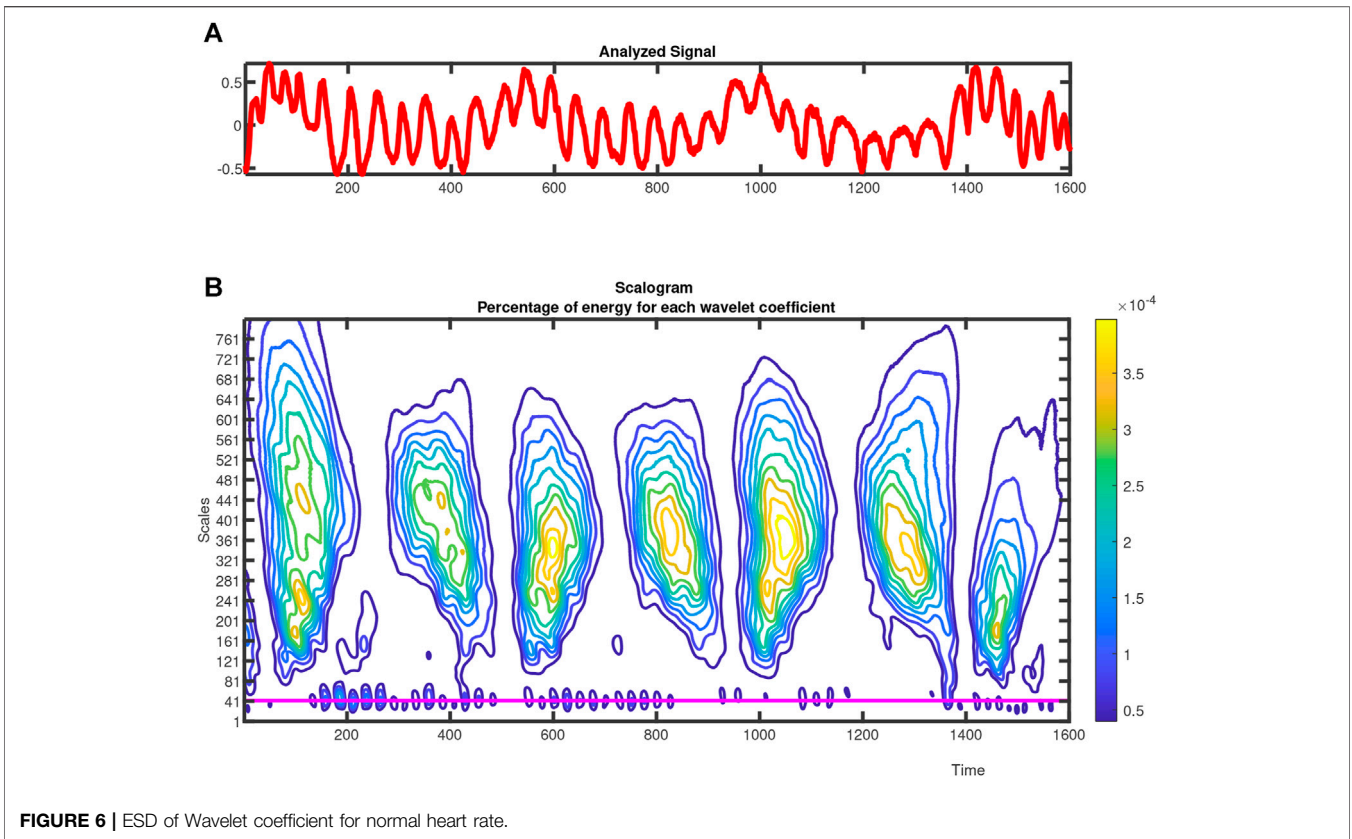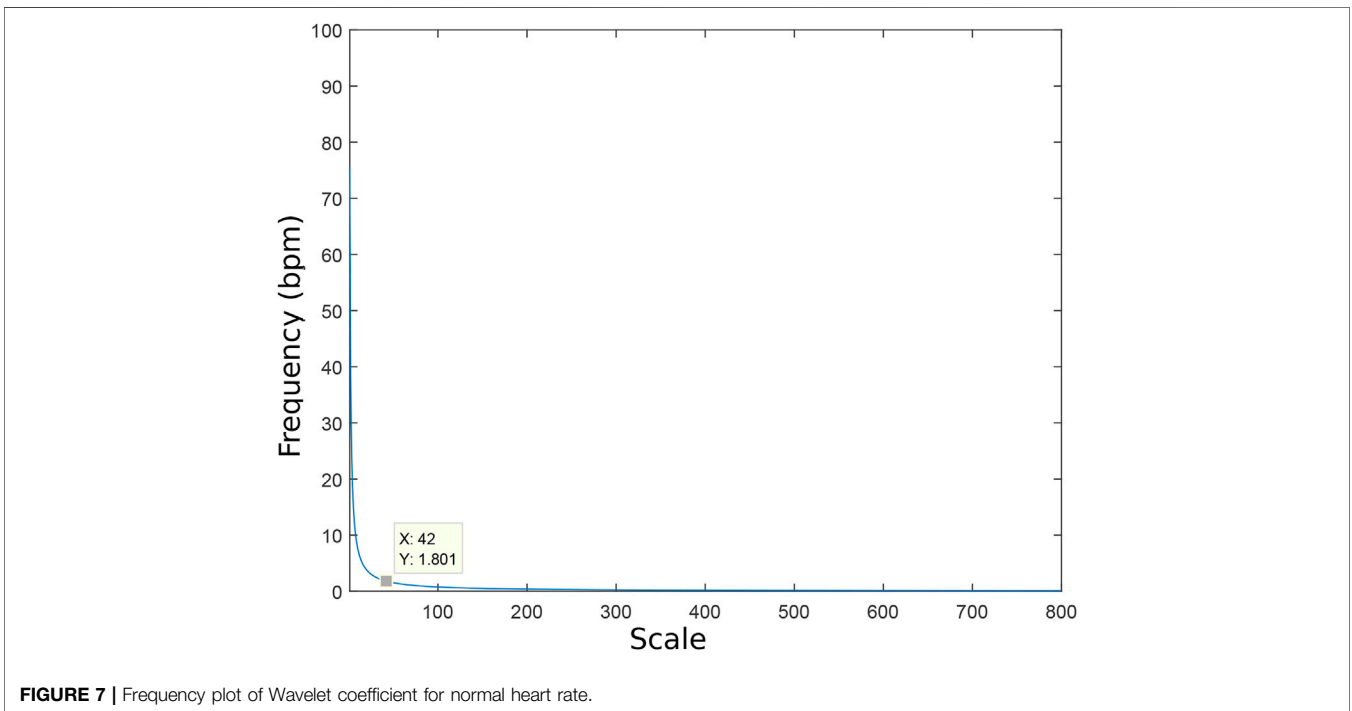**FIGURE 6 |** ESD of Wavelet coefficient for normal heart rate.

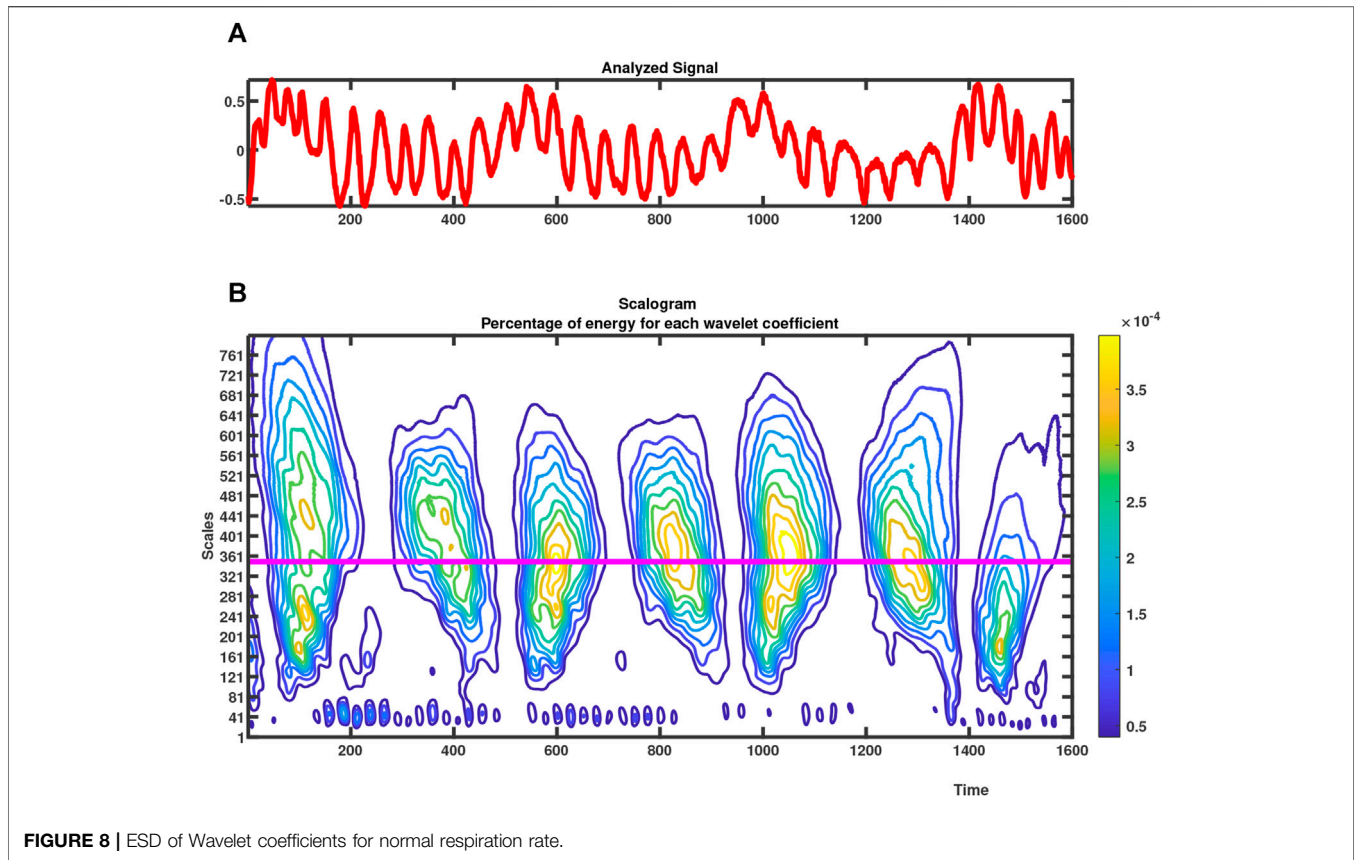**FIGURE 7 |** Frequency plot of Wavelet coefficient for normal heart rate.

FIGURE 8 | ESD of Wavelet coefficients for normal respiration rate.

TABLE 1 | Respiration rate comparison.

Description	Scale value for respiration rate	Scale to frequency correspondence for respiration rate	Respiration rate = 60*Frequency (bpm)	Relative percentage error
Actual	350	0.2161	12.966	___
Lossy	345	0.2193	13.158	1.48%
AR-based model	348	0.2174	13.044	0.57%
ARMA model	349	0.2167	13.002	0.28%

TABLE 2 | Heart rate comparison.

Description	Scale value for heart-rate	Scale to frequency corresponding to heart-rate	Heart rate = 60*Frequency (bpm)	Relative percentage error
Actual	42	1.801	108.06	___
Lossy	39	1.94	116.4	7.14%
AR-based model	40	1.891	113.46	4.99%
ARMA model	41	1.845	110.7	2.44%

Hence, this information would work as a benchmark for a particular patient. In this work, we have used ECG sensor; which is current gold standard in monitoring heart rate (Nelson and Allen, 2019), for comparison of the results. The respiration was monitored manually to find the actual breathing rate of the human.

So far, we have considered the normal situation wherein complete data is received from patients under investigation for analysis purposes. In the unique approach used in this article, we have generated simulation results for comparison in this section. However, in real life, data may not be available smoothly for a number of reasons, including Radar Cross

Section (RCS) issues or congestion of buffer which is often used for storage purposes. In such cases, it is important to design a remedy to cure this critical issue. This paper aims to address this situation by proposing a data loss recovery scheme embedded with vital signs implemented by the Wavelet transform.

5 CONSEQUENCES OF DATA LOSS

In the previous section, the importance of vital sign and its monitoring tool (WT) has been elaborated for uninterrupted data. In the next section, vital signs are monitored when the received data is incomplete for any practical reason (e.g. CSR area, channel or buffer congestion, sensor fault and/or failure, etc.). It is necessary to deal with this, otherwise it can lead to serious consequences, especially in terms of human casualty. The received data is random and overall 50 samples are lost.

The data with intermittent samples has been analyzed and is shown in **Supplementary Figure S2** (upper sub-figure) where the interruption can be viewed by a circle in the initial phase. The Wavelet coefficients generated from the interrupted analyzing signal can be seen in the lower sub-figure of **Supplementary Figure S2**. The energy associated with heart rate (low assembled energy line) corresponds to a scale-factor of 39 which is shown by a pink continuous line.

From the scale to the frequency **Supplementary Figure S3**, the corresponding frequency of the 39 scale-factor is 1.94 Hz. The equivalent heart rate is $1.94 \times 60 = 116.4$ bpm (beats/min). Therefore, the data loss has led to a noticeable misunderstanding, which may offer hindrance effects, specifically in the medical treatment of a patient. The deviation resulted by the data-loss is 7.71%.

From the same interrupted analyzing signal, the maximum energy for high dense coefficients correspond to 345 scale factor which is shown by a pink continues line in **Supplementary Figure S4**. Transforming these coefficients to scale-to-frequency mapping results in a frequency of 0.2193 Hz as shown in **Supplementary Figure S5**. The respiration rate computed from this would be $0.2193 \times 60 = 13.158$ rpm (respiration/minute). The percent deviation of respiration rate from the normal reading is 1.48%.

Once again, the intermittent observations have caused a drift in readings of the respiration rate. In the subsequent section, we provide a remedy for the loss of data and its effect in vital sign monitoring has been provided.

6 ANALYSIS AFTER RECOVERY OF DATA LOSS THROUGH AR-BASED MODEL

In this section, the analyzing signal which was subjected to data loss earlier has been recovered through AR-based series and then employed in vital signs monitoring. This recovered analyzing signal is shown in **Supplementary Figure S6** (Upper sub-figure). In the next stages, the Wavelet coefficients are achieved for respiration and heart rates from this recovered analyzing signal.

The Wavelet coefficients show a scale of 40 for heart rate as shown in **Supplementary Figure S6**. Planting these coefficients to

scale-frequency mapping results in a frequency of 1.891 Hz which is shown in **Supplementary Figure S7**. The heart rate computed from this is $1.891 \times 60 = 113.46$ bpm (beats/minute). The amount of deviation by this reading from the uninterrupted reading would be 4.99%.

Which is almost 30.11% recovery compared to the results with lossy data. For the same recovered analyzing signal through AR based series depicted in **Supplementary Figure S8** (upper sub-figure). The maximum energy for high dense coefficients correspond to coefficients at 348 scale which is shown by a pink continues line at the bottom depicted in **Supplementary Figure S8** (lower sub-figure). Transforming these coefficients to scale to frequency mapping would produce a frequency of 0.2174 Hz shown in **Supplementary Figure S9**. The respiration rate computed from this reading is 0.2174*60 = 13.04 bpm (breath/minute). The degree of deviation by this reading from uninterrupted reading would be 0.57%, which is almost 60% recovery compared to the results with loss.

This paper aims to improve the results obtained in this section, by introducing ARMA based recovery as discussed earlier in **Section 3**. Using this novel approach, improvement in accuracy is expected at the cost of computational efforts.

7 ANALYSIS AFTER RECOVERY OF DATA LOSS THROUGH ARMA-BASED MODEL

It is believed that using more information (input and measure signal), more accurate data can be reconstructed. Hence, the recovery made through ARMA based model where both signals are employed should generate more efficient results than AR-based model, where only the measurement vector is used in the recovery.

In this section, using the concept of the ARMA-based model, the intermittent analyzing signal is first recovered, then the two critical information is obtained. This recovered signal is shown in **Supplementary Figure S10** (upper sub-figure). In the next phase, the Wavelet coefficients are achieved for respiration and heart rates from this recovered analyzing signal. The Wavelet coefficients reflect a scale of 41 for heart rate shown in **Supplementary Figure S10** (lower sub-figure). Transforming these coefficients to scale to frequency mapping results in a frequency of 1.845 Hz shown in **Supplementary Figure S11**. The heart rate computed from this scale is $1.845 \times 60 = 110.7 bpm$ (beats/minute). The level of deviation by this reading from the uninterrupted reading would be 2.44%, which is approximately 66% recovery compared to the results with lossy data. Through the same strategy, the maximum energy-column comprising of high dense coefficients associate a scale value of 349 which is depicted by the continues line in **Supplementary Figure S12**. Substituting these coefficients into scale-frequency mapping show a frequency of 0.2167 Hz (**Supplementary Figure S13**). The respiration rate computed from this is 0.2167*60 = $13.002 bpm$ (breath/minute). The degree of deviation of this reading from benchmark reading would be 0.28%, which is 80.28% recovery compared to results with data loss.

To summarize, four compact scenarios have been compiled for monitoring of vital signs, namely;

1. When normal data arrives (without any loss).
2. When there is random data loss.
3. When the data is recovered through AR-based model (existing method)
4. When data is recovered through ARMA-based model (proposed technique)

A total of 50 samples are manually lost at a particular location. Although various scenarios may be introduced and described through this case study. In this paper, a chunk of data, collectively at one location is considered to be lost. **Table 1** and **Table 2** summarize the performance of two algorithms (existing AR-based model and proposed ARMA-based model) for the respiration and heart rates, respectively. As can be viewed from the last row of the two tables, the proposed ARMA-based model efficiently reproduced the lost information and the vital signs (the two rates) are very much close to actual readings. Hence it results in minimum error.

CONCLUSION

In this paper, vital signs monitoring has been considered for practically achieved data. Due to its direct link with human beings, the importance of vital signs is very clear. The loss of such information needs to be efficiently handled in order to avoid catastrophic results. Initially, the vital signs are monitored from normal data, where there is no data loss. This provides a benchmark to perform comparison for later stages where measurement data is intermittent in nature after striking the patient. This lossy data has been observed in vital sign monitoring (heart and respiration rates) with degrading outcomes. This data loss is then attempted to be recovered through the AR-based model which gives much better results compared to lossy results. However, the AR-based model entertained only the measurement vector in the recovery process. An improved version is introduced in this paper, which implies both measurement vector and input data in the recovery phase. After recovery, when implanted in the vital sign monitoring, the simulation results show that more efficient and closer to actual data is obtained through this scheme. In other words, the reproduced data is less affected by data-loss which is verified by vital sign monitoring results.

It can be concluded that, if any data has a certain level of a trend in its structure, the data can be reproduced through the AR-based or ARMA-based model. If not, then piece-wise similarity may be assumed in the recovery process. It is necessary to mention that both AR and ARMA-based models are computationally expensive. In future, non-stationary attitude may be investigated in the same context as it could give further insights into the problem.

DATA AVAILABILITY STATEMENT

The raw data supporting the conclusion of this article will be made available by the authors, without undue reservation.

AUTHOR CONTRIBUTIONS

NK designed the experiments, wrote the paper and supervised the algorithm development. SS worked on the implementation of algorithms. IA and FK (1st author) helped in experiments to design and write the manuscript. FK (5th author) participated in data collection and paper writing.

FUNDING

SUPPLEMENTARY MATERIAL

The Supplementary Material for this article can be found online at: https://www.frontiersin.org/articles/10.3389/frsip.2021.742441/full#supplementary-material

Supplementary Figure S1 | Frequency plot of Wavelet coefficients for normal respiration rate.

Supplementary Figure S2 | ESD of Wavelet coefficients for heart rate (Lossy Data).

Supplementary Figure S3 | Frequency plot of Wavelet coefficients for heart rate (Lossy Data).

Supplementary Figure S4 | ESD of Wavelet coefficients for respiration rate (Lossy data).

Supplementary Figure S5 | Frequency plot of Wavelet coefficients for respiration rate (Lossy data).

Supplementary Figure S6 | ESD of Wavelet coefficients for heart rate (AR-based approach).

Supplementary Figure S7 | Frequency plot for Wavelet coefficients for heart rate (AR-based approach).

Supplementary Figure S8 | ESD of Wavelet coefficients for respiration rate (AR-based approach).

Supplementary Figure S9 | Frequency plot of Wavelet coefficients for respiration rate (AR-based model).

Supplementary Figure S10 | ESD of Wavelet coefficients for heart rate (ARMA-based approach).

Supplementary Figure S11 | Frequency plot for Wavelet coefficients for heart rate (ARMA-based approach).

Supplementary Figure S12 | ESD of Wavelet coefficients for respiration rate (ARMA-based approach).

Supplementary Figure S13 | Frequency plot of Wavelet coefficients for respiration rate (ARMA-based model).

REFERENCES

Andersen, N., Granhaug, K., Michaelsen, J. A., Bagga, S., Hjortland, H. A., Knutsen, M. R., et al. (2017). A 118-mw Pulse-Based Radar Soc in 55-nm Cmos for Non-Contact Human Vital Signs Detection. *IEEE J. Solid-State Circuits* 52, 3421–3433. doi:10.1109/jssc.2017.2764051

Briso, C., Calvo, C., and Xu, Y. (2019). Uwb Propagation Measurements and Modelling in Large Indoor Environments. *IEEE Access* 7, 41913–41920. doi:10.1109/access.2019.2905142

Buehrer, R. M., Davis, W. A., Safaai-Jazi, A., and Sweeney, D. (2003). "Characterization of the Ultra-Wideband Channel," in IEEE Conference on Ultra Wideband Systems and Technologies, Reston, VA, 26–31. doi:10.1109/UWBST.2003.1267796

Cardillo, E., Li, C., and Caddemi, A. (2021). Vital Sign Detection and Radar Self-Motion Cancellation through Clutter Identification. *IEEE Trans. Microwave Theor. Techn.* 69, 1932–1942. doi:10.1109/tmtt.2021.3049514

Chia, M. Y. W., Leong, S. W., Sim, C. K., and Chan, K. M. (2005). "Through-wall UWB Radar Operating within FCC's Mask for Sensing Heart Beat and Breathing Rate," in European Radar Conference, Paris, France, 267. doi:10.1109/EUMC.2005.1610358

Chóliz, J., Hernández, Á., and Valdovinos, A. (2011). A Framework for Uwb-Based Communication and Location Tracking Systems for Wireless Sensor Networks. *Sensors* 11, 9045–9068. doi:10.3390/s110909045

Cramer, R. J.-M., Scholtz, R. A., and Win, M. Z. (2002). Evaluation of an Ultra-Wide-Band Propagation Channel. *IEEE Trans. Antennas Propagat.* 50, 561–570. doi:10.1109/tap.2002.1011221

Fear, E. C., Li, X., Hagness, S. C., and Stuchly, M. A. (2002). Confocal Microwave Imaging for Breast Cancer Detection: Localization of Tumors in Three Dimensions. *IEEE Trans. Biomed. Eng.* 49, 812–822. doi:10.1109/tbme.2002.800759

Fernandes, J. R., and Wentzloff, D. (2010). "Recent Advances in Ir-Uwb Transceivers: An Overview," in Proceedings of 2010 IEEE International Symposium on Circuits and Systems, Paris, France, 3284–3287. doi:10.1109/ISCAS.2010.5537916

Fontana, R. J. (2004). Recent System Applications of Short-Pulse Ultra-Wideband (Uwb) Technology. *IEEE Trans. Microwave Theor. Techn.* 52, 2087–2104. doi:10.1109/tmtt.2004.834186

Grewal, M., and Andrews, A. (2001). *Kalman Filtering: Theory and Practice Using MATLAB*. Hoboken, New Jersey: John Wiley & Sons.

Gu, C., Wang, G., Inoue, T., and Li, C. (2013). "Doppler Radar Vital Sign Detection with Random Body Movement Cancellation Based on Adaptive Phase Compensation," in IEEE MTT-S International Microwave Symposium Digest (MTT), Seattle, WA, 1–3. doi:10.1109/mwsym.2013.6697618

Khan, F., and Cho, S. (2017). A Detailed Algorithm for Vital Sign Monitoring of a Stationary/Non-Stationary Human through IR-UWB Radar. *Sensors* 17, 290. doi:10.3390/s17020290

Khan, F., Ghaffar, A., Khan, N., and Cho, S. H. (2020). An Overview of Signal Processing Techniques for Remote Health Monitoring Using Impulse Radio Uwb Transceiver. *Sensors* 20, 2479. doi:10.3390/s20092479

Khan, F., Leem, S. K., and Cho, S. H. (2018). Human-Computer Interaction Using Radio Sensor for People with Severe Disability. *Sensors Actuators A: Phys.* 282, 39–54. doi:10.1016/j.sna.2018.08.051

Khan, N., Fekri, S., and Gu, D. (2010). Improvement on State Estimation for Discrete-Time Lti Systems with Measurement Loss. *Measurement* 43, 1609–1622. doi:10.1016/j.measurement.2010.09.011

Khan, N., Khan, K., Khan, A., Alam, I., Khan, F. U., Khan, S. U., et al. (2019). Accommodate Data Loss in Monitoring Vital Signs through Autoregressive Model. *J Med. Imaging Hlth Inform.* 9, 1205–1214. doi:10.1166/jmihi.2019.2712

Khan, N., Khattak, M. I., Khan, M. N., Khan, F., Khan, L. U., Salam, S. A., and Gu, D.-W. (2013). "Implementation of Linear Prediction Techniques in State Estimation," in Proceedings of 2013 10th International Bhurban Conference on Applied Sciences Technology (IBCAST), Islamabad, Pakistan, 77–83. doi:10.1109/IBCAST.2013.6512134

Lazaro, A., Girbau, D., and Villarino, R. (2009). Wavelet-Based Breast Tumor Localization Technique Using a Uwb Radar. *Prog. Electromagnetics Res.* 98, 75–95. doi:10.2528/pier09100705

Le, M. (2020). Heart Rate Extraction Based on Eigenvalues Using Uwb Impulse Radar Remote Sensing. *Sensors Actuators A: Phys.* 303, 111689. doi:10.1016/j.sna.2019.111689

Li, B., Zhou, Z., Zou, W., Li, D., and Zhao, C. (2010). Optimal Waveforms Design for Ultra-Wideband Impulse Radio Sensors. *Sensors* 10, 11038–11063. doi:10.3390/s101211038

Liu, H., Allen, J., Zheng, D., and Chen, F. (2019). Recent Development of Respiratory Rate Measurement Technologies. *Physiol. Meas.* 40, 07TR01–28. doi:10.1088/1361-6579/ab299e

Nelson, B. W., and Allen, N. B. (2019). Accuracy of Consumer Wearable Heart Rate Measurement during an Ecologically Valid 24-Hour Period: Intraindividual Validation Study. *JMIR Mhealth Uhealth* 7, e10828. doi:10.2196/10828

Oziel, M., Korenstein, R., and Rubinsky, B. (2017). Radar Based Technology for Non-Contact Monitoring of Accumulation of Blood in the Head: A Numerical Study. *PLOS ONE* 12, e0186381–20. doi:10.1371/journal.pone.0186381

Shen, H., Xu, C., Yang, Y., Sun, L., Cai, Z., Bai, L., et al. (2018). Respiration and Heartbeat Rates Measurement Based on Autocorrelation Using Ir-Uwb Radar. *IEEE Trans. Circuits Syst.* 65, 1470–1474. doi:10.1109/tcsii.2018.2860015

Sifuzzaman, M., Islam, M. R., and Ali, M. Z. (2009). Application of Wavelet Transform and its Advantages Compared to Fourier Transform. *J. Phys. Sci.* 13, 121–134.

Staderini, E. M. (2002). Uwb Radars in Medicine. *IEEE Aerosp. Electron. Syst. Mag.* 17, 13–18. doi:10.1109/62.978359

Tariq, A., Zahid, A., Khan, U., Khan, N., and Khan, F. (2017). "Implementation of Wavelet Transform for Monitoring of Vital Signs through Ir-Uwb Radar," in 2017 International Conference on Communication, Computing and Digital Systems (C-CODE), Islamabad, Pakistan, 337–340. doi:10.1109/C-CODE.2017.7918953

Thiel, F., Kosch, O., and Seifert, F. (2010). Ultra-Wideband Sensors for Improved Magnetic Resonance Imaging, Cardiovascular Monitoring and Tumour Diagnostics. *Sensors* 10, 10778–10802. doi:10.3390/s101210778

Wang, G. R., Han, H. G., Kim, S. Y., and Kim, T. W. (2017). Wireless Vital Sign Monitoring Using Penetrating Impulses. *IEEE Microw. Wireless Compon. Lett.* 27, 94–96. doi:10.1109/lmwc.2016.2630001

Yang, X., Zhang, X., Qian, H., Ding, Y., and Zhang, L. (2020). "Mmt-Hear: Multiple Moving Targets Heartbeats Estimation and Recovery Using Ir-Uwb Radars," in 42nd Annual International Conference of the IEEE Engineering in Medicine and Biology Society (EMBC), Montreal, QC, 5733–5736. doi:10.1109/EMBC44109.2020.9175318